Ocean Sci. Discuss., 10, 261–290, 2013
www.ocean-sci-discuss.net/10/261/2013/
doi:10.5194/osd-10-261-2013
© Author(s) 2013. CC Attribution 3.0 License.

Ocean Science
Discussions
Open Access

This discussion paper is/has been under review for the journal Ocean Science (OS).
Please refer to the corresponding final paper in OS if available.

Discussion Paper | Discussion Paper | Discussion Paper | Discussion Paper |

An optical model for deriving the spectral particulate backscattering coefficients in clear and turbid coastal waters

S. P. Tiwari and P. Shanmugam

Department of Ocean Engineering, Indian Institute of Technology Madras,
Chennai-600036, India

Received: 26 October 2012 – Accepted: 16 January 2013 – Published: 4 February 2013

Correspondence to: P. Shanmugam (pshanmugam@iitm.ac.in)

Published by Copernicus Publications on behalf of the European Geosciences Union.

Abstract

An optical model is developed based on the diffuse attenuation coefficient (K_d) to estimate particulate backscattering coefficients $b_{bp}(\lambda)$ in clear and turbid coastal waters. A large in-situ data set is used to establish robust relationships between $b_{bp}(530)$ and $b_{bp}(555)$ and $K_d(490)$ using an efficient nonlinear least square method which uses the Trust-Region algorithm with Bisquare weights scheme to adjust the coefficients. These relationships are obtained with good correlation coefficients ($R^2 = 0.786$ and 0.790), low Root Mean Square Error (RMSE = 0.00076 and 0.00072) and 95 % confidence bounds. The new model is tested with two independent data sets such as the NOMAD SeaWiFS Match-ups and OOXIX IOP algorithm workshop evaluation data set (Version 2.0w APLHA). Results show that the new model makes good retrievals of b_{bp} at all key wavelengths (from 412–683 nm), with statistically significant improvements over other inversion models. Thus, the new model has the potential to improve our knowledge of particulate matters and their optical variability in both clear and turbid coastal waters.

1 Introduction

Knowledge of light scattering and absorption properties of the seawater constituents is very important to understand spectral reflectance and its variability (Gordon et al., 1975). Among these properties, spectral particulate backscattering $b_{bp}(\lambda)$ has scientific implications and practical applications in optical remote sensing, as the light backscattered from various seawater constituents provides possibility to derive information on the particulate populations under investigation (Shanmugam et al., 2011). The particulate backscattering mainly depends on the particle size distribution (PSD), shape, index of refraction, and structure (homogeneous, multi-layers, etc.). Measurements of these parameters are extremely difficult and most of the existing techniques for determination of the PSD often do not provide measures of the contribution of submicron particles, which are suspected to dominate particulate backscattering (Antoine et al.,

Discussion Paper | Discussion Paper | Discussion Paper | Discussion Paper |

OSD

10, 261–290, 2013

Spectral particulate backscattering coefficients

S. P. Tiwari and P. Shanmugam

CC BY

2011; Morel and Ahn, 1991; Stramski and Kiefer, 1991). The fraction of b_{bp} affects the ocean colour, determined by the relative contribution of living and nonliving particles (such as inorganic minerals, phytoplankton, and organic detritus) (Gordon et al., 1975). In open ocean waters, most of the scattering covaries with the phytoplankton concentration. However, in coastal waters the scattering property is determined by particles derived from the river advection, waves and currents, local biogenic production, and atmospheric deposition. These sources display significant spatial and temporal variations in the particulate populations, and therefore the corresponding variations in ocean colour. However, our present knowledge of these variations in scattering properties of the particulate load (e.g. suspended sediments, phytoplankton blooms, detritus, composition and size) (van de Hulst, 1981) in coastal waters under investigation remains poorly understood (Shanmugam et al., 2011).

Many empirical and semi-analytical algorithms have been developed in the recent decades (Gordon et al., 1988; Garver and Siegel, 1997; Carder et al., 1999; IOCCG, 2006) to estimate particulate backscattering coefficients from remote sensing data. The empirical algorithms are generally derived from the relationship of irradiance reflectance or remote sensing reflectance and backscattering coefficients, These algorithms give better estimates of $b_{bp}(\lambda)$ in clear ocean waters, but produce large errors in coastal waters (with high mineral particle concentrations). The Mie theory implementation is also limited by the lack of knowledge on the imaginary part of refractive index and assumption of the same particle size distribution for organic and inorganic fractions of seawater (Stramski et al., 2001; Twardowski et al., 2001; Risovic, 2002; Babin et al., 2003; Green et al., 2003). Semi-analytical models are based on radiative transfer theory (Maritorena et al., 2002), and can be applied to a wide range of the ocean environments. Recently, commercial instruments (e.g. AC-S, BB9 (WET Labs Inc.)) have become available for direct measurements of scattering and backscattering properties. Unfortunately, practical difficulties are associated with these instruments for direct measurements of the volume scattering function (VSF) at sufficient angular and spectral ranges (Chami et al., 2006).

OSD
10, 261–290, 2013

The objectives of this work are to develop a robust model to estimate spectral particulate backscattering coefficients in clear and turbid coastal waters, to evaluate its performance using independent in-situ data and SeaWiFS satellite match-ups from a variety of waters, and to compare its results with those of the global inversion models (IOCCG, 2006).

2 Data and method

In-situ data

The NASA bio-Optical Marine Algorithm Dataset (NOMAD) – a global, high-quality in-situ data highly suitable for algorithm development and validation (Werdell and Bailey, 2005) was obtained from the NASA SeaWiFS Bio-optical Archive and Storage System (SeaBASS). This data set contains coincident measurements of b_b, Chl, R_{rs} (λ), K_d and other data collected simultaneously in various regional and global waters. It also contains concurrent SeaWiFS remote sensing reflectances (R_{rs}) and in-situ b_b at several key wavelengths. A subset of NOMAD in-situ data was made of co-located b_b (for several wavelengths between 405 and 683 nm) and corresponding remote sensing reflectances ($N = 331$, hereafter referred as NOMAD-A). The satellite match-ups consisted of 74 valid data points for both b_b and R_{rs} at the SeaWiFS wavebands (referred as NOMAD-B).

The NOMAD-SeaWiFS match-ups and OOXIX IOP algorithm workshop evaluation data (Version 2.0w APLHA) were used as independent data sets (after eliminating certain data common to NOMAD-A) for validating the new model in the context of remote-sensing applications (Werdell and Bailey, 2005; Werdell, 2009; Brewin et al., 2011). The later data set consisted of 185 matched remote sensing reflectances at SeaWiFS wavebands and in-situ particulate backscattering coefficients (hereafter referred as NOMAD-C data). For the NOMAD data set, the particulate backscattering $b_{bp}(\lambda)$ values were obtained according to $b_{bp}(\lambda) = b_b(\lambda) - b_{bw}(\lambda)$, where $b_{bw}(\lambda)$ is the

OSD
10, 261–290, 2013

S. P. Tiwari and P. Shanmugam

backscattering coefficient of pure sea-water obtained from Smith and Baker (1981). Figure 1 shows the histograms of b_{bp} (λ) data at 530 and 555 nm and K_d at 490 nm for a wide range of waters. The low-high values of the histograms correspond to clear waters to turbid coastal waters.

3 Model Description

3.1 Particulate backscattering coefficient – background

The backscattering coefficient (b_b) is an inherent optical property (IOP) (Preisendorfer, 1961) which is defined as a function of the volume scattering function (VSF), β (λ, θ). It describes the scattered radiant intensity into a scattering angle θ per unit irradiance of the incident unpolarized beam of the light per unit volume of water (Mobley, 1994, 1995). The integration of β (λ, θ) (VSF with units $m^{-1}\,sr^{-1}$ where θ is the scattering angle and λ the wavelength) over the backward hemisphere provides the backscattering coefficient through the following expression,

$$b_b(\lambda) = 2\pi \int_{\pi/2}^{\pi} \beta(\lambda,\theta)\sin(\lambda)\mathrm{d}\theta \tag{1}$$

This approach is not often used because it requires detailed scattering information over a wide range, and the instrumentation is not yet commercially available to carry out such measurements in the ocean environment. Combination of randomly oriented molecules, marine inorganic and organic (living or nonliving) particles, and bubbles in seawater contributes to b_b. However, determination of how the relative contributions of these components vary as a function of the physical and bio-optical state of oceanic waters remains an elusive task (Stramski et al., 2004).

OSD
10, 261–290, 2013

S. P. Tiwari and P. Shanmugam

The total backscattering coefficient $b_b(\lambda)$ is the sum of the backscattering by pure water b_{bw} (λ) and particulate backscattering b_{bp} (λ).

$$b_b(\lambda) = b_w(\lambda) + b_{bp}(\lambda) \tag{2}$$

Hence, backscattering by particles b_{bp} can be described as follows,

$$b_{bp}(\lambda) = b_b(\lambda) - b_{bw}(\lambda) \tag{3}$$

where the scattering coefficient of pure seawater (b_w) is obtained from Smith and Baker (1981) to derive the backscattering by pure seawater ($b_{bw} = b_w/2$).

In the recent decades, many laboratory and field investigations yielded robust constraints on the absorption basis function spectral variations (Roesler et. al., 2003). Since backscattering sensors are relatively new, there is less information on backscattering basis functions. Previous studies by Morel and Ahn (1991) and Stramski and Kiefer (1991) demonstrated that most of the backscattering (70–90 %) in ocean waters is caused by particles smaller than 1 µm. In fact, Mie theory was used to compute optical properties of particles (for absorbing spheres) which yielded strong spectral features near the absorption peaks (van de Hulst, 1957; Gordon, 1974; Bricaud and Morel, 1986; Zaneveld and Kitchen, 1995). However, there was difficulty in constraining these features which led to the implementation of Mie theory for populations of non-absorbing homogeneous spheres, in which b_{bp} was expressed as a smoothly varying function (Morel, 1973). Thus, the particulate backscattering b_{bp} (λ) can be defined as:

$$b_{bp}(\lambda) = b_{bp}(\lambda_r) \times \left(\frac{555}{\lambda}\right)^Y \tag{4}$$

where $b_{bp}(\lambda)$ and $b_{bp}(\lambda_r)$ are the particulate backscattering coefficient at a desired wavelength and a reference wavelength, respectively. Y is the spectral slope that determines variability, shape, and magnitude of the particulate backscattering spectra. Most of the inversion models use the Eq. (4) with slight modification for retrieval of the particulate backscattering coefficients from satellite ocean colour data.

OSD
10, 261–290, 2013

3.2 Modelling particulate backscattering coefficient

For deriving the particulate backscattering coefficients, some studies showed good correlation between b_{bp} and R_{rs} and others found better correlations between b_{bp} and chlorophyll (Chl) or suspended sediment (SS) concentration (Boss et al., 2009a; Sun et al., 2009; Martinez-Vicente et al., 2010). It should be noted that these relationships are not always consistent due to the lack of a theoretical framework for predicting b_{bp}. Our present understanding of major contributions to b_{bp} in natural waters is therefore uncertain, and it is unknown that which particles backscatter light most efficiently (Stramski et al., 2004). Mie calculations (for scattering) suggest that significant contributions to b_{bp} come from submicron particles (Stramski and Kiefer, 1991), but there is evidence that application of this theory is inadequate for computation of b_{bp} for particle assemblages in natural waters (Bohren and Singham, 1991; Kitchen and Zenveld, 1992; Clavano et al., 2007). Thus, the current inversion models are limited to relatively clear ocean waters because of their difficulty in determining b_{bp} features (i.e. spectral signature and magnitude) in turbid coastal waters (Shanmugam et al., 2011). This prevents our knowledge of b_{bp} and thus interpretation of ocean colour signals (Antoine et al., 2011). In order to obtain more accurate b_{bp} values, new models with better parameterizations are needed to derive b_{bp} features over the entire visible wavelength domain.

The spectral diffuse attenuation coefficient $K_d(\lambda)$ is one of the most important apparent optical property (AOP) (Preisendorfer, 1976) of seawater, directly linked to the IOPs such as absorption and backscattering properties (Sathyendranath and Platt, 1988; Gordon, 1989; Lee et al., 2005a,b). This optical property is indicative of how strongly light at a particular wavelength is attenuated within the water column, thus it has wide applicability in ocean optics. It plays a very critical role to understand the absorption and backscattering properties, photosynthesis and primary productivity models (Platt, 1986; Sathyendranath, 1989), heat budgets (Lewis, 1990; Morel, 1994), other biological processes in the water column, and to classify water types (Jerlov, 1976).

OSD
10, 261–290, 2013

cc BY

The nonlinear least square method is better suited to fit a nonlinear model to data. This type of model is defined by an equation that is nonlinear in the coefficients or a combination of linear and nonlinear in the coefficients. Mathematically, the nonlinear model is given by the formula $z = f(\chi, \gamma) + \varepsilon$, where z is the response, and can be derived using a set of coefficients (γ) and variable quantity (χ) with an approximate error value (ε). Linear models are easy to solve using the simple mathematical regression analysis, while nonlinear models are more difficult to fit; thus an iterative method is used to determine the required coefficients to obtain the desired response including the approximate error value. The fitted response value $\hat{z} = f(\chi, p)$ is produced after the successive iterative process to produce a new set of coefficients (p) and reduce residual between the data and the fitted curve, until the fit reaches the specified convergence criteria, which involves the calculation of the Jacobian of $f(\chi, p)$, which is defined as a matrix of partial derivatives taken with respect to the coefficients.

In this study, a suitable K_d-based model is developed to derive $b_{bp}(\lambda)$ in the entire visible wavelength (400 nm to 700 nm) domain. To estimate slope values and b_{bp} at a reference wavelength, the relationships of $K_d(490)$ versus b_{bp} (530) and (555) are obtained using the NOMAD-A bio-optical data set. The power function is fitted to this in-situ data using the non-linear least-square method, with good correlation coefficients ($R^2 = 0.786$ for b_{bp} (530) versus $K_d(490)$ and $R^2 = 0.790$ for $b_{bp}(555)$ versus $K_d(490)$), very small RMSE values (0.00076 and 0.00072 respectively), and 95 % confidence bounds (Fig. 2). The best-fit power equations coefficients are achieved using the Trust-region method along with Bisquare weights scheme to adjust the coefficients for a better fit, as it can solve difficult nonlinear problems more efficiently than the other methods (Coleman et al., 1996). The Bisquare weights scheme is used because it is very useful to minimize the effect of outliers. The Mueller (2000) model is then used to

OSD
10, 261–290, 2013

Spectral particulate backscattering coefficients

S. P. Tiwari and P. Shanmugam

CC BY

estimate K_d at 490 nm. Consequently the following equations are obtained:

$$K_d(490) = 0.016 + 0.1365 \left(\frac{R_{rs}(490)}{R_{rs}(555)} \right)^{-1.54} \quad (5)$$

$$b_{bp}(530) = -0.000162 + 0.0309 \times (K_d(490))^{1.15}; R^2 = 0.7857 \quad (6)$$

$$b_{bp}(555) = -0.000157 + 0.0304 \times (K_d(490))^{1.109}; R^2 = 0.7902 \quad (7)$$

The values of Y are derived from the above Eqs. (6) and (7) of the b_{bp} (530) and b_{bp} (555) as follows,

$$\text{Slope } Y = \frac{\log_{10}[b_{bp}(530)/b_{bp}(555)]}{\log_{10}[555/530]} \quad (8)$$

The derived Y values are applicable to both clear and turbid ocean waters, where these values vary from 0.7089 to 1.7082 with the average value of 1.130. The calculated values of b_{bp} at the reference wavelength of 555 nm and Y values from Eqs. (7) and (8) can be substituted in Eq. (4) to estimate b_{bp} (λ) coefficients in the entire visible wavelength domain.

4 Performance assessment

The accuracy of the model is assessed by comparing its predicted $b_{bp}(\lambda)$ values with in-situ $b_{bp}(\lambda)$ data. Two basic statistical measures are used such as the root mean square error (RMSE) and mean relative error (MRE). The accuracy of $b_{bp}(\lambda)$ predictions is also assessed based on the slope (S), intercept (I), and correlation coefficient (R^2) of the linear regression between the in-situ and predicted b_{bp} (λ) values. Systematic and random errors are calculated by the MRE and RMSE, respectively (IOCCG, 2006);

OSD
10, 261–290, 2013

CC BY

these metrics are defined as:

$$\mathrm{RMSE} = \left(\frac{\sum_{i=1}^{N} \left[\log\left(b_{\mathrm{bp}_i}^{\mathrm{model}}\right) - \log\left(b_{\mathrm{bp}_i}^{\mathrm{insitu}}\right) \right]^2}{N-2} \right)^{1/2} \tag{9}$$

$$\mathrm{MRE} = \sum_{i=1}^{N} \frac{\log\left(b_{\mathrm{bp}_i}^{\mathrm{model}}\right) - \log\left(b_{\mathrm{bp}_i}^{\mathrm{insitu}}\right)}{\log\left(b_{\mathrm{bp}_i}^{\mathrm{insitu}}\right)} \times 100\,\% \tag{10}$$

where $b_{\mathrm{bp}_i}^{\mathrm{model}}$ stands for the model derived values, $b_{\mathrm{bp}_i}^{\mathrm{insitu}}$ stands for the in-situ measurements, and N is the number of valid retrievals. Tables 1, 2 and 3 summarize the statistical analyses results of the model validation with known $b_{\mathrm{bp}}(\lambda)$ data.

5 Results

The performance of the new model for predicting $b_{\mathrm{bp}}(\lambda)$ values was evaluated with three data sets: NOMAD-A data (used for the model parameterization at two wavelengths 530 and 555 nm) at the wavelengths 412–683 nm, independent NOMAD-B data (SeaWiFS satellite match-ups) at the wavelengths 412–555 nm, and NOMAD-C data at the wavelengths 412–555 nm. The results of the new model are also compared with those of the other inversion models (e.g. LM, QAA, and GSM semi-analytical models). The statistical evaluation results of these models are summarized in Tables 1, 2, and 3. To gain further insight into their performances, scatterplots of the model $b_{\mathrm{bp}}(\lambda)$ values versus in-situ $b_{\mathrm{bp}}(\lambda)$ values are shown at the key wavelengths in Figs. 3–8.

OSD
10, 261–290, 2013

5.1 Spectral variability of the particulate backscattering coefficient

A large set of the particulate backscattering spectra was generated by the present model, with the varying spectral slope values that influence on the shape and magnitude of spectral b_{bp} (λ) curves, and compared with the corresponding in-situ spectra (NOMAD-A) at the selected wavelengths (Fig. 3). The spectral comparison is interesting as the shape and magnitude of the modelled spectral b_{bp} (λ) curves are consistent with those of the in-situ spectral b_{bp} (λ) curves. It is observed that the b_{bp} values are strong in the blue (e.g. 412 and 443 nm) domain and decrease towards the longer wavelengths. The difference between modelled and in-situ spectra is small and confined to a few observations made in particle-loaded waters. Such a small deviation of the model results may arise from the inadequate range of the slope coefficients to account for different compositions of the particulate materials. The difference may also be caused by the bottom influence and /or sea state conditions.

5.2 Model validation

Figure 4 shows the scatterplots of the model-derived $b_{bp}(\lambda)$ values versus in-situ $b_{bp}(\lambda)$ values at the key wavelengths (including red wavelengths) and the corresponding statistical evaluation results are summarized in Table 1. Note that the $b_{bp}(\lambda)^{insitu}$ and $b_{bp}(\lambda)^{model}$ coefficients are highly correlated (close to the 1 : 1 line) indicating that the agreement between them is very good at 412, 443, 490, 510, 530, 555, 670, and 683 nm with small statistical errors (note that other inversion models do not provide $b_{bp}(\lambda)$ values at the red wavelengths). These results reveal that $b_{bp}(\lambda)$ values predicted by the new model at these wavelengths match with their corresponding in-situ $b_{bp}(\lambda)$ values well. Figure 5 provides a better clarity in the variations of RMSE and MRE (%) of the new model at different wavelengths (412–683). The percentile MRE values are very small for the NOMAD-A data set, with the maximum value at 412 nm (∼ 0.45 %) and the minimum value at 683 nm (∼ −0.33 %). The model yields relatively high RMSE at

CC BY

412 nm and low RMSE at 530 and 555 nm. Overall (average), the model gives excellent statistics for the NOMAD-A data set (RMSE ~ 0.1413 and MRE ~ 0.0937 %).

5.3 Inter-comparison with other inversion models

In order to inter-compare the results of new model with those of the existing inversion models (Garver-Siegel-Maritorena model – GSM, Quasi-Analytical Algorithm – QAA, and Constrained Linear-Matrix inversion model – CLM), all four models were applied to the independent NOMAD-B (NOMAD SeaWiFS match-ups) and NOMAD-C (OOXIX IOP Algorithm Workshop data) data sets. Figure 6 shows that the $b_{bp}(\lambda)$ spectra (shape and magnitude) derived from the new model are similar to the in-situ $b_{bp}(\lambda)$ spectra, although showing slight differences with in-situ b_{bp} at the selected wavelengths. By contrast, other inversion models tend to distort the spectral shape and magnitude of $b_{bp}(\lambda)$ to a noticeable extent. GSM model produces increasingly high b_{bp} values at the green wavelengths compared to the other two models. Overall, the new model provides accurate $b_{bp}(\lambda)$ values in both clear and turbid coastal waters, therefore enabling us to extend it for application to the ocean colour remote sensing applications.

Figure 7 shows the comparison of model-predicted $b_{bp}(\lambda)$ values versus in-situ values (NOMAD-B) for the selected wavelengths (412, 443, 490, 510 and 555 nm). Table 2 presents the results of statistical analysis for all the models. It is observed that b_{bp} (λ) values derived from the QAA and GSM models are fairly linearly correlated with the in-situ $b_{bp}(\lambda)$ values at all five wavelengths, although producing significant underestimations or overestimations across the range of $b_{bp}(\lambda)$ values at these wavelengths. On the contrary, $b_{bp}(\lambda)$ values are significantly underestimated by the LM model (at the lower end of b_{bp} at these wavelengths) for this data set. As a result, the errors associated with this model are very high compared to those with the GSM and QAA models (Table 2). However, the LM model performs fairly well at higher $b_{bp}(\lambda)$ values (coastal waters). When the new model was applied to the same data sets, it can be seen that the $b_{bp}(\lambda)$ values are more realistic (aligned more closely to the 1 : 1 line) without much overestimation and underestimation. This indicates relatively good agreement between

OSD
10, 261–290, 2013

CC BY

the modelled $b_{bp}(\lambda)$ and in-situ $b_{bp}(\lambda)$ values at 412, 443, 490, 510, and 555 nm. The statistical evaluation results also show that the overall performance of the new model is good at the five SeaWiFS wavebands.

Further validation with the NOMAD-C (OOXIX IOP Algorithm Workshop) data set was performed to assess the efficiency of these models. The results of this validation are shown in Fig. 8 and Table 3, where similar trends in $b_{bp}(\lambda)$ retrievals are observed with the other inversion models despite their errors being considerably low for this data set (except QAA model which caused more scattering of data between predicted and in-situ $b_{bp}(\lambda)$ with the increased errors). By contrast, the new model outperforms these inversion models in terms of producing accurate $b_{bp}(\lambda)$ values (close agreement with in-situ $b_{bp}(\lambda)$ values as indicated by the data around the 1 : 1 line) at 412, 443, 490, 510, and 555 nm with low statistical errors (Table 3). These results confirm the potential of the new model to produce $b_{bp}(\lambda)$ values in a wide range of waters.

6 Discussion and conclusion

The importance of the particulate backscattering coefficients in ocean colour remote sensing has been discussed and emphasized in the previous studies (Hoge et al., 1996; Loisel and Stramski, 2000; Maritorena et al., 2002; Lee et al., 2002; Boss and Roesler, 2005; Wang et al., 2006; Smyth et al., 2006; Pinkerton et al., 2006; Gordon et al., 2009; Antoine et al., 2011; Shanmugam et al., 2011). Though several models are available to retrieve $b_{bp}(\lambda)$ as the function of chlorophyll concentration or spectral remote sensing reflectance, none of these models provide $b_{bp}(\lambda)$ values over the entire visible spectral bands that are available with satellite sensors such as SeaWiFS, MODIS and MERIS. Furthermore, none of these models provide accurate $b_{bp}(\lambda)$ values, even in the blue-green wavelengths, in turbid coastal waters (Shanmugam et al., 2011). This is perhaps due to improper parameterizations and inadequate $b_{bp}(\lambda)$ measurements in a variety of waters covering a large geographical extent. As a consequence, very little information is available on the b_{bp} spectral variability (shape and magnitude). One of the differences with other inversion models is the input parameter. The new model makes use of $K_d(490)$ as an input parameter which can be easily estimated from satellite ocean colour measurements. The non-linear least square approach that does not require any assumption on the spectral shapes of absorption, scattering, and backscattering is identified as one of the best methods to accurately predict the $b_{bp}(\lambda)$ spectral variability from the estimated $K_d(490)$. A set of equations that relate AOPs to IOPs is derived and tested using independent in-situ data and SeaWiFS satellite match-ups data. In this study, $K_d(490)$ is found to be an appropriate proxy to predict the $b_{bp}(\lambda)$, which increases the accuracy of $b_{bp}(\lambda)$ predictions with the new model in both clear and coastal waters.

The inter-comparison results based on the above independent data sets are interesting that the new model provide the statistically improved $b_{bp}(\lambda)$ products (at selected wavelengths) compared to other inversion models (GSM, QAA and LM). Among these three inversion models, GSM and QAA models give $b_{bp}(\lambda)$ values better consistent with in-situ data, while LM model shows poor performance at the selected wavelengths. Nevertheless, the new model outperforms these inversion models in terms of providing accurate $b_{bp}(\lambda)$ values over the visible wavelength domain (400–700 nm), and thus it has wide applicability in both clear and turbid coastal waters.

The present study is expected to form the basis for robust relationships between $b_{bp}(\lambda)$ and K_d in a wide range of coastal and open ocean waters. More measurements of these optical properties in typical coastal waters will allow the refinement of the new model which can be used to derive information on the refractive index and particle size distribution based on certain optical models to study the particle populations and their characteristics in coastal waters. The results discussed in this paper have important implications for ocean colour remote sensing.

OSD
10, 261–290, 2013

CC BY

Acknowledgements. This work was supported by grants from the NRB (Project Number OEC1112106NRBXPSHA). This work was also supported by the MHRD, Government of India and Indian Institute of Technology Madras. The authors would like to thank the NASA Ocean Biology Processing Group for making available the global, high quality bio-optical (NOMAD) data set to this study. We are grateful to the reviewers for their valuable comments, which helped to improve the structure and content of this paper.

References

Antonie, D., Siegal, D. A., Kostadinov, T., Maritorena, S., Nelson, N. B., Gentilli, B., Vellucci, V., and Guillocheau N.: Variability in optical particle backscattering in contrasting bio-optical oceanic regimes, Limnol. Oceanogr., 56, 955–973, 2011.

Babin, M., Morel, A., Fournier-Sicre, V., Fell, F., and Stramski, D.: Light scattering properties of marine particles in coastal and oceanic waters as related to the particle mass concentration, Limnol. Oceanogr., 48, 843–859, 2003b.

Bohren, C. F. and Singham, S. B.: Backscattering by nonspherical particles: a review of methods and suggested new approaches, J. Geophys. Res., 96, 5269–5277, 1991.

Boss, E. and Roesler, C.: Over constrained linear matrix inversion with statistical selection, Remote Sensing of Inherent Optical Properties: Fundamentals, Tests of Algorithms, and Applications, edited by: Lee, Z., IOCCG, Dartmouth, NS, Canada, IOCCG Rep. 5, 2006.

Boss, E., Taylor, L., Gilbert, S., Gundersen, K., Hawley, N., Janzen, C., Johengen,T., Purcell, H., Robertson, C., Schar, D. W. H., Smith, G. J., and Tamburri, M. N.: Comparison of inherent optical properties as a surrogate for particulate matter concentration in coastal waters, Limnol. Oceanogr.-Meth., 7, 803–810, 2009.

Brewin, R. J. W., Devred, E., Sathyendranath, S., Lavender, S. J., and Hardman-Mountford, N. J.: Model of phytoplankton absorption based on three size classes, Appl. Optics, 50, 4535–4549, 2011.

Bricaud, A. and Morel, A.: Light attenuation and scattering by a phytoplanktonic cells: a theoretical modeling, Appl. Optics, 25, 571–580, 1986.

Coleman, T. F. and Li, Y.: An interior, trust region approach for nonlinear minimization subject to bounds, SIAM J. Optimiz., 6, 418–445, 1996.

CC BY

Carder, K. L., Chen, F. R., Lee, Z. P., Hawes, S. K., and Kamykowski, D.: Semianalytic Moderate-Resolution Imaging Spectrometer algorithms for chlorophyll-*a* and absorption with bio-optical domains based on nitrate depletion temperatures, J. Geophys. Res., 104, 5403–5421, 1999.

Chami, M., Shybanov, E. B., Khomenko, G. A., Lee, M. E. G., Martynov, O. V., and Korotaev, G. K.: Spectral variation of the volume scattering function measured over the full range of scattering angles in a coastal environment, Appl. Optics 45, 3605–3619, 2006.

Clavano, W. R., Boss, E., and Karp-Boss, L.: Inherent optical properties of non-spherical marine-like particles – from theory to observations, Oceanogr. Mar. Biol., 45, 1–38, 2007.

Garver, S. A. and Siegel, D.: Inherent optical property inversion of ocean colour spectra and its biogeochemical interpretation – 1. Time series from the Sargasso Sea, J. Geophys. Res., 102, 18607–18625, 1997.

Gordon, H. R.: Spectral variations in the volume scattering function at large angles in natural waters, J. Opt. Soc. Am., 64, 773–775, 1974.

Gordon, H. R.: A semi-analytic radiance model of ocean colour, J. Geophys. Res., 93, 10909–10924, 1988.

Gordon, H. R.: Dependence of the diffuse reflectance of natural waters on the sun angle, Limnol. Oceanogr., 34, 1389–1409, 1989.

Gordon, H. R., Brown, O. B., and Jacobs, M. M.: Computed relationships between the inherent and apparent optical properties of a flat homogeneous ocean, Appl. Optics, 14, 2417–2427, 1975.

Gordon, H. R., Lewis, M. R., McLean, S. D., Twardowski, M. S., Freeman, S. A., Voss, K. J., and Boynton, G. C.: Spectra of particulate backscattering in natural waters, Opt. Express, 17, 16192–16208, 2009.

Green, R. E., Sosik, H. M., Olson, R. J., and DuRand, M. D.: Flow cytometric determination of size and complex refractive index for marine particles: comparison with independent and bulk estimates, Appl. Optics, 42, 526–541, 2003.

Hoge, F. E. and Lyon, P. E.: Satellite retrieval of inherent optical properties by linear matrix inversion of oceanic radiance models: an analysis of model and radiance measurement errors, J. Geophys. Res.-Oceans, 101, 16631–16648, 1996.

Jerlov, N. G.: Marine Optics, Elsevier, Amsterdam, 1976.

Kitchen, J. C. and Zaneveld, J. R. V.: A three-layered sphere model of the optical properties of phytoplankton, Limnol. Oceanogr., 37, 1680–1690, 1992.

Lee, Z. P., Carder, K. L., and Arnone, R. A.: Deriving inherent optical properties from water colour: a multiband quasi-analytical algorithm for optically deep waters, Appl. Optics 41, 5755–5772, 2002.

Lee, Z. P., Du, K. P., and Arnone, R.: A model for the diffuse attenuation coefficient of downwelling irradiance, J. Geophys. Res., 110, C02016, doi:10.1029/2004JC002275, 2005a.

Lee, Z. P., Darecki, M., Carder, K. L., Devis, C. O., Stramski, D., and Rhea, W. J.: Diffuse attenuation coefficient of downwelling irradiance: an evaluation of remote sensing methods, J. Geophys. Res., 110, C02017, doi:10.1029/2004JC002573, 2005b.

Lewis, M. R., Carr, M., Feldman, G., Esaias, W., and McMclain, C.: Influence of penetrating solar radiation on the heat budget of the equatorial pacific ocean, Nature, 347, 543–545, 1990.

Loisel, H. and Stramski, D.: Estimation of the inherent optical properties of natural waters from the irradiance attenuation coefficient and reflectance in the presence of Raman scattering, Appl. Optics, 39, 3001–3011, 2000.

Maritorena, S., Siegel, D. A., and Peterson, A. R.: Optimization of a semianalytical ocean colour model for global-scale applications, Appl. Optics, 41, 2705–714, 2002.

Martinez-Vicente, V., Land, P. E., Tilstone, G. H., Widdicombe, C., and Fishwick, J. R.: 2010. Particulate scattering and backscattering related to water constituents and seasonal changes in the Western English Channel, J. Plankton Res., 32, 603–619, 2010.

Mobely, C. D.: Light and water. Radiative transfer in natural waters, San Diego, Academic Press, 1994.

Mobely, C. D.: The optical properties of water, in: Handbook of Optics, Fundamental, Techniques, and Design, vol. 1, edited by: Bass, M., Van Stryland, E. W., Williams, D. R., and Wolf, W. L., McGraw-Hill, New York, 43.3–43.56, 1995.

Morel, A.: Diffusion de la lumière par les eaux de mer: Résultats experimentaux et approach théoretique, in: AGARD Lecture Series, 3.1.1–3.1.76, 1973.

Morel, A. and Ahn, Y. H.: Optics of heterotrophic nanoflagellates and ciliates. A tentative assessment of their scattering role in oceanic waters compared to those of bacterial and algal cells, J. Mar. Res., 49, 177–202, 1991.

Morel, A. and Antoine, D.: Heating rate within the upper ocean in relation to its bio-optical state, J. Phys. Oceanogr., 24, 1652–1665, 1994.

Mueller, J. L.: SeaWiFS algorithm for the diffuse attenuation coefficient, *K* (490), using water-leaving radiances at 490 and 555 nm, in SeaWiFS Postlaunch Calibration and Validation

Analyses, part 3, edited by: Hooker, S. B., 24–27, NASA Goddard Space Flight Cent., Greenbelt, Md., 2000.
Pinkerton, M. H., Moore, G. F., Lavender, S. J., Gall, M. P., Oubelkheir, K., Richardson, K. M., Boyd, P. W., and Aiken, J.: A method for estimating inherent optical properties of New Zealand continental shelf waters from satellite ocean colour measurements, New Zeal J. Mar. Fresh., 40, 227–247, 2006.
Platt, T.: Primary production of ocean water column as a function of surface light intensity: algorithms for remote sensing, Deep Sea Res. 33, 149–163, 1986.
Preinsendorper, R. W.: Application of radiative transfer theory to light measurements in the sea, Monogr. Int. Union Geod. Geophys., Paris, 10, 11–30, 1961.
Preisendorfer, R. W.: Hydrologic Optics, vol. 1, Introduction, Natl. Tech. Inf. Serv., Springfield, Va, 1976.
Risovic, D.: Effect of suspended particulate-size distribution on the backscattering ratio in the remote sensing of seawater, Appl. Optics, 41, 7092–7101, 2002.
Roesler, C. S. and Boss, E.: Spectral beam attenuation coefficient retrieved from ocean colour inversion, Geophys. Res. Lett., 30, 1468, doi:10.1029/2002GL016185, 2003.
Sathyendranath, S. and Platt, T.: The spectral irradiance field at the surface and in the interior of the ocean: a model for applications in oceanography and remote sensing, J. Geophys. Res., 93, 9270–9280, 1988.
Sathyendranath, S., Prieur, L., and Morel, A.: A three-component model of ocean colour and its application to remote sensing of phytoplankton pigments in coastal waters, Int. J. Remote Sens., 10, 1373–1394, 1989.
Shanmugam, P., Sundarbalan, B., Ahn, Y. H., and Ryu, J. H.: A new inversion model to retrieve the particulate backscattering in coastal oceans, IEEE T. Geosci. Remote, 49, 2463–2475, 2011.
Smith, R. C. and Baker, K. S.: Optical properties of the clearest natural waters, Appl. Optics, 20, 177–184, 1981.
Smyth, T. J., Moore, G. F., Hirata, T., and Aiken, J.: Semianalytical model for the derivation of ocean colour inherent optical properties: description, implementation, and performance assessment, Appl. Optics, 46, 429–430, 2006.
Stramski, D. and Kiefer, K. A.: Light scattering by microorganisms in the open sea, Prog. Oceanogr., 28, 4 343–4383, 1991.

OSD
10, 261–290, 2013

Spectral particulate backscattering coefficients

S. P. Tiwari and P. Shanmugam

CC BY

Stramski, D., Bricaud, A., and Morel, A.: Modeling the inherent optical properties of the ocean based on the detailed composition of planktonic community, Appl. Optics, 40, 2929–2945, 2001.

Stramski, D., Boss, E., Bogucki, D., and Voss, K. J.: The role of seawater constituents in light backscattering in the ocean, Prog. Oceanogr., 61, 27–56, 2004.

Sun, D., Li, Y., Wang, Q., Gao, J., Lv, H., Le, C., and Huang, C.: Light scattering properties and their relation to biogeochemical composition in a turbid productive lake: Lake Taihu case study, Appl. Optics, 48, 1979–1989, 2009.

Twardowski, M., Boss, E., Macdonald, J. B., Pegau, W. S., Barnard, A. H., and Zaneveld, V. J. R.: A model for estimating bulk refractive index from the optical backscattering ratio and the implications for understanding particle composition in case I and case II waters, J. Geophys. Res., 106, 14129–14142, 2001.

Van de Hulst, H. C.: Light Scattering by Small Particles, John Wiley, New York, 1957.

Van de Hulst H. C.: Light Scattering by Small Particles, Dover Publications, 1981.

Victor, M. V., Land, P. E., Tilstone, G. H., Widdicombe, C. and Fishwick, J. R.: Particulate scattering and backscattering related to water constituents and seasonal changes in the Western English Channel, J. Plankton Res., 32, 603–629, 2010.

Wang, P., Boss, E. S., and Roesler, C. S.: Uncertainties of inherent optical properties obtained from semianalytical inversions of ocean colour, Appl. Optics, 44, 4074–4085, 2005.

Werdell, P. J. and Bailey, S. W.: An improved in-situ bio-optical data set for ocean colour algorithm development and satellite data product validation, Remote Sens. Environ., 98, 122–140, 2005.

Werdell, P. J., Bailey, S. W., Franz, B. A., Harding Jr., L. W., Feldman, G. C., and McClain, C. R.: Regional and seasonal variability of chlorophyll *a* in Chesapeake Bay as observed by SeaWiFS and MODIS-Aqua, Remote Sens. Environ., 113, 1319–1330, 2009.

Zaneveld, J. R. V. and Kitchen, J. C.: The variation in the inherent optical properties of phytoplankton near an absorption peak as determined by various models of cell structure, J. Geophys. Res., 100, 13309–13320, 1995.

OSD

10, 261–290, 2013

CC BY

Table 1. Statistical comparisons between the modelled and known particulate backscattering $b_{bp}(\lambda)$ values (NOMAD- A in-situ data). RMSE, MRE, BIAS and linear-regression results for the SeaWiFS bands centered at 412, 443, 490, 510, 530, 555, 670, and 683 nm.

IOP	RMSE	MRE(%)	BIAS	Slope	Intercept	R^2	N
			NOMAD-A				
$b_{bp}(412)$	0.1555	0.45	0.0113	0.6594	−0.8522	0.7072	331
$b_{bp}(443)$	0.1486	0.37	0.0096	0.686	−0.7974	0.7367	331
$b_{bp}(490)$	0.141	0.23	0.0059	0.7153	−0.7387	0.7692	331
$b_{bp}(510)$	0.1387	0.17	0.0046	0.7256	−0.7183	0.7797	331
$b_{bp}(530)$	0.1369	0.11	0.0028	0.7337	−0.7033	0.7883	331
$b_{bp}(555)$	0.1354	0.04	0.0012	0.7421	−0.688	0.7963	331
$b_{bp}(670)$	0.137	−0.29	−0.008	0.7585	−0.6736	0.81	331
$b_{bp}(683)$	0.1379	−0.33	−0.0091	0.7585	−0.6765	0.8097	331
Average	0.1413	0.0937	0.0022	0.7223	−0.731	0.7746	331

OSD
10, 261–290, 2013

Table 2. Statistical comparisons between the modelled (predicted by using the satellite SeaWiFS remote sensing reflectance) and NOMAD-B in-situ data. RMSE, MRE, BIAS and linear-regression results for the SeaWiFS bands centered at 412, 443, 490, 510, and 555 nm.

IOP	RMSE	MRE(%)	BIAS	Slope	Intercept	R^2	N
			NM				
$b_{bp}(412)$	0.1852	−0.1	−0.0025	0.4782	−1.2914	0.4806	74
$b_{bp}(443)$	0.1806	−0.31	−0.0077	0.5032	−1.2492	0.5049	74
$b_{bp}(490)$	0.1768	−0.75	−0.0192	0.5328	−1.2035	0.5315	74
$b_{bp}(510)$	0.1759	−0.86	−0.022	0.5427	−1.1887	0.5403	74
$b_{bp}(555)$	0.176	−1.17	−0.0306	0.5595	−1.1683	0.554	74
Average	0.1789	−0.638	−0.0164	0.5232	−1.2202	0.5222	74
			LM				
$b_{bp}(412)$	0.4109	−11.94	−0.3348	0.9357	−0.4937	0.5203	74
$b_{bp}(443)$	0.418	−11.99	−0.3406	0.9255	−0.5268	0.5055	74
$b_{bp}(490)$	0.4312	−12.18	−0.3515	0.9016	−0.6009	0.4787	74
$b_{bp}(510)$	0.435	−12.17	−0.3536	0.888	−0.6392	0.4658	74
$b_{bp}(555)$	0.4448	−12.23	−0.3597	0.8548	−0.7347	0.4368	74
Average	0.4279	−12.102	−0.348	0.9011	−0.599	0.4814	74
			QAA				
$b_{bp}(412)$	0.2524	−4	−0.1029	0.2931	−1.8491	0.2227	74
$b_{bp}(443)$	0.2228	−2.51	−0.0644	0.3462	−1.6984	0.3132	74
$b_{bp}(490)$	0.1937	−0.59	−0.0152	0.4227	−1.4788	0.4345	74
$b_{bp}(510)$	0.1869	0.24	0.0061	0.4525	−1.3907	0.474	74
$b_{bp}(555)$	0.1834	1.91	0.1091	0.5148	−1.2045	0.5369	74
Average	0.2078	−0.99	−0.0134	0.4058	−1.5243	0.3962	74
			GSM				
$b_{bp}(412)$	0.2447	−7.31	−0.1947	0.7606	−0.7862	0.6908	74
$b_{bp}(443)$	0.1983	−5.06	−0.1332	0.7603	−0.7323	0.6873	74
$b_{bp}(490)$	0.1578	−2.01	−0.052	0.7517	−0.6814	0.6732	74
$b_{bp}(510)$	0.1522	−0.7	−0.018	0.7451	−0.6684	0.6648	74
$b_{bp}(555)$	0.1658	2.02	0.0511	0.7265	−0.6551	0.6425	74
Average	0.1837	−2.612	−0.0693	0.7488	−0.7046	0.6717	74

OSD
10, 261–290, 2013

Table 3. Statistical comparisons between the modelled and NOMAD-C in situ data. RMSE, MRE, BIAS and linear-regression results for the SeaWiFS bands centered at 412, 443, 490, 510, and 555 nm.

IOP	RMSE	MRE(%)	BIAS	Slope	Intercept	R^2	N
			NM				
$b_{bp}(412)$	0.1268	−1.15	−0.0287	0.709	−0.7507	0.7214	185
$b_{bp}(443)$	0.1213	−0.95	−0.0242	0.7297	−0.7056	0.7499	185
$b_{bp}(490)$	0.117	−0.85	−0.022	0.7493	−0.6667	0.7781	185
$b_{bp}(510)$	0.1159	−0.75	−0.0195	0.7537	−0.6583	0.7861	185
$b_{bp}(555)$	0.1158	−0.64	−0.0169	0.7583	−0.6543	0.7965	185
Average	0.11936	−0.868	−0.02226	0.74	−0.68712	0.7664	185
			LM				
$b_{bp}(412)$	0.3352	−8.77	−0.2385	1.3386	0.6016	0.6683	185
$b_{bp}(443)$	0.3272	−8.51	−0.2343	1.347	0.6405	0.6954	185
$b_{bp}(490)$	0.319	−8.25	−0.2312	1.3428	0.6506	0.7234	185
$b_{bp}(510)$	0.3146	−8.07	−0.2278	1.3347	0.6404	0.7308	185
$b_{bp}(555)$	0.3076	−7.78	−0.2225	1.3107	0.5969	0.7411	185
Average	0.3207	−8.276	−0.2308	1.3347	0.626	0.7118	185
			QAA				
$b_{bp}(412)$	0.2127	−2.21	−0.056	0.3227	−1.7366	0.2506	185
$b_{bp}(443)$	0.1875	−0.56	−0.0141	0.4164	−1.4852	0.3821	185
$b_{bp}(490)$	0.1685	1.58	0.0399	0.5414	−1.1396	0.5473	185
$b_{bp}(510)$	0.1681	2.49	0.063	0.5872	−1.0076	0.6003	185
$b_{bp}(555)$	0.1788	4.32	0.1091	0.6781	−0.7398	0.6883	185
Average	0.1831	1.124	0.0283	0.5091	−1.2217	0.4937	185
			GSM				
$b_{bp}(412)$	0.2257	−6.31	−0.1671	1.0051	−0.1546	0.7086	185
$b_{bp}(443)$	0.1725	−3.63	−0.0949	1.0085	−0.0734	0.7351	185
$b_{bp}(490)$	0.1363	0.05	0.0013	1.0013	0.0048	0.7614	185
$b_{bp}(510)$	0.1406	1.61	0.0412	0.9939	0.0254	0.7683	185
$b_{bp}(555)$	0.1806	4.88	0.1227	0.973	0.0515	0.7771	185
Average	0.1711	−0.68	−0.0193	0.9963	−0.0292	0.7501	185

OSD
10, 261–290, 2013

CC BY

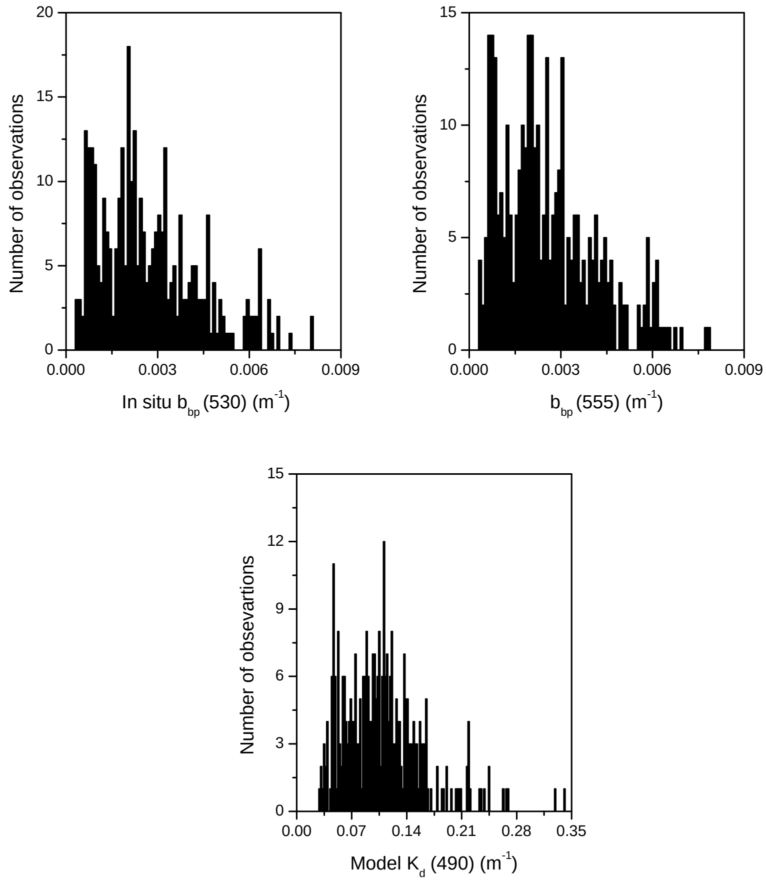

Fig. 1. Histogram of the particulate backscattering (b_{bp}) coefficients at 530 and 55 nm (top panels) and the diffuse attenuation coefficients K_d(490) (bottom panel) from the NOMAD-A in-situ data (N = 331).

OSD
10, 261–290, 2013

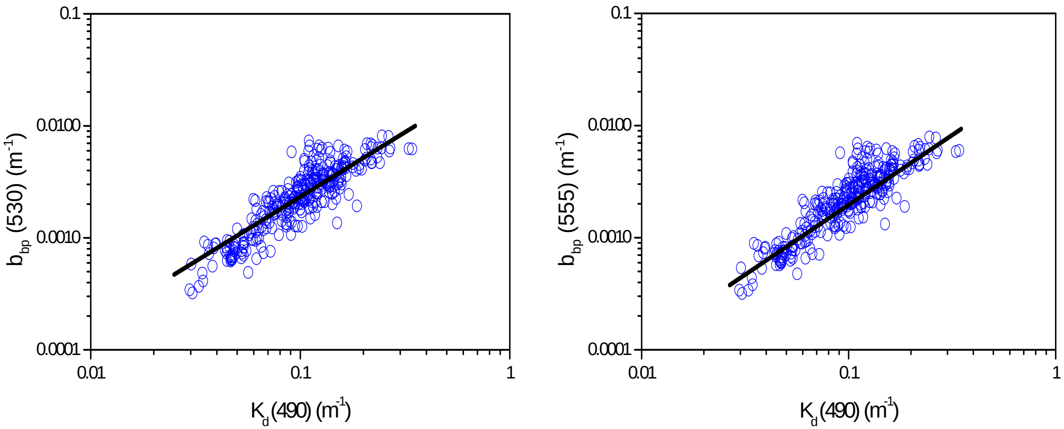

Fig. 2. Relationships between the $b_{bp}(530)$ and $b_{bp}(555)$ and diffuse attenuation coefficient $K_d(490)$ from the NOMAD-A in-situ data set ($N = 331$).

CC BY

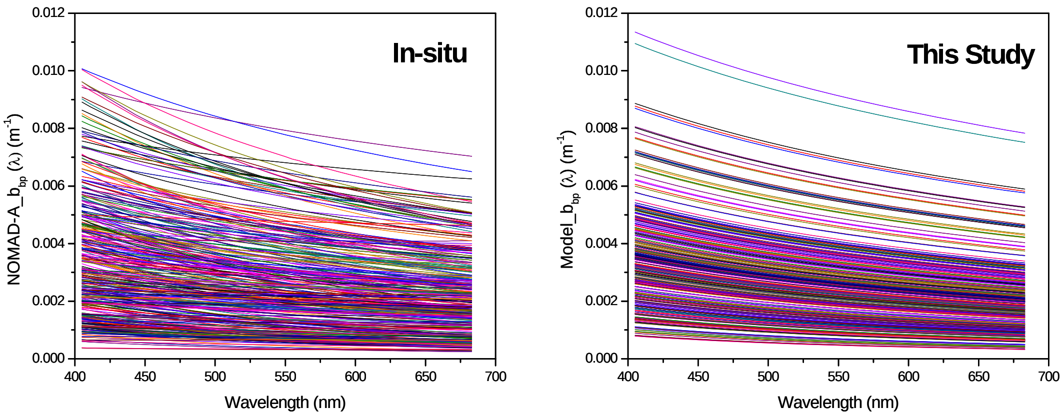

Fig. 3. Spectral variations in the particulate backscattering spectra $b_{bp}(\lambda)$ (m^{-1})) from the NOMAD-A in-situ data (left panel) and new model (right panel).

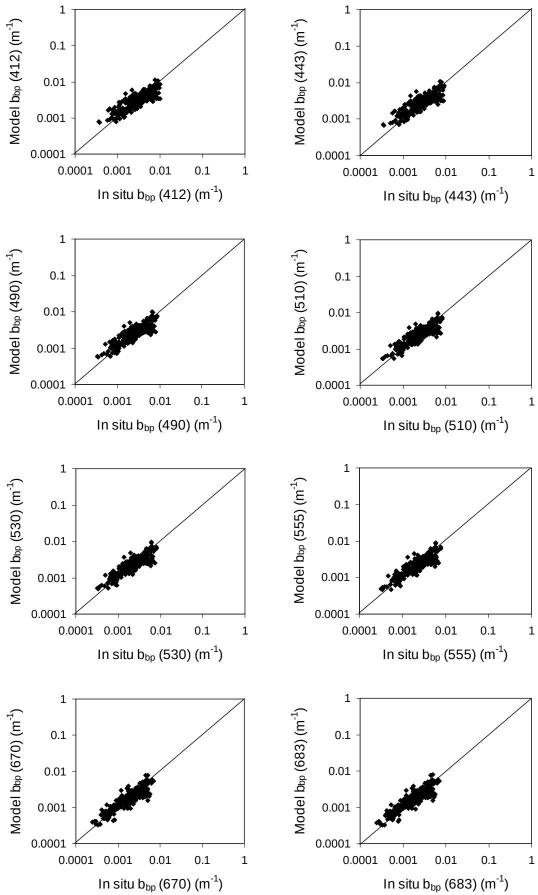

Fig. 4. Comparison between the in-situ b_{bp} (NOMAD-A) and model b_{bp} (m^{-1}) at 412, 443, 490, 510, 530, 555, 670, and 683 nm ($N = 331$).

OSD
10, 261–290, 2013

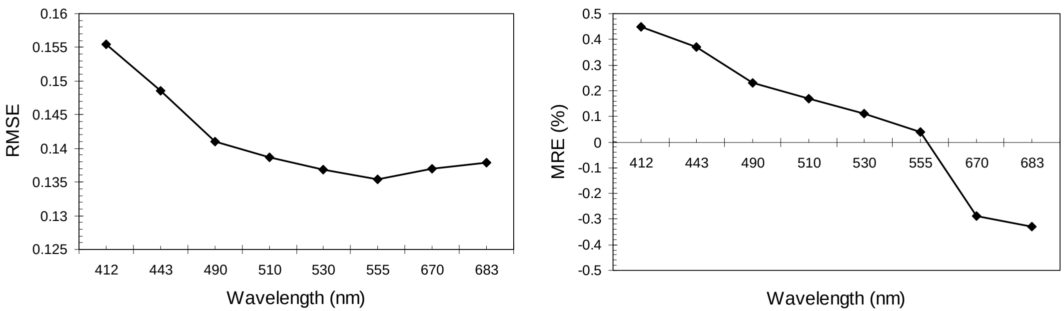

Fig. 5. RMSE and MRE (%) between the derived and NOMAD-A in-situ data (N = 331) of the particulate backscattering coefficient (b_{bp}) (m^{-1}) for the new model.

OSD
10, 261–290, 2013

Spectral particulate backscattering coefficients

S. P. Tiwari and P. Shanmugam

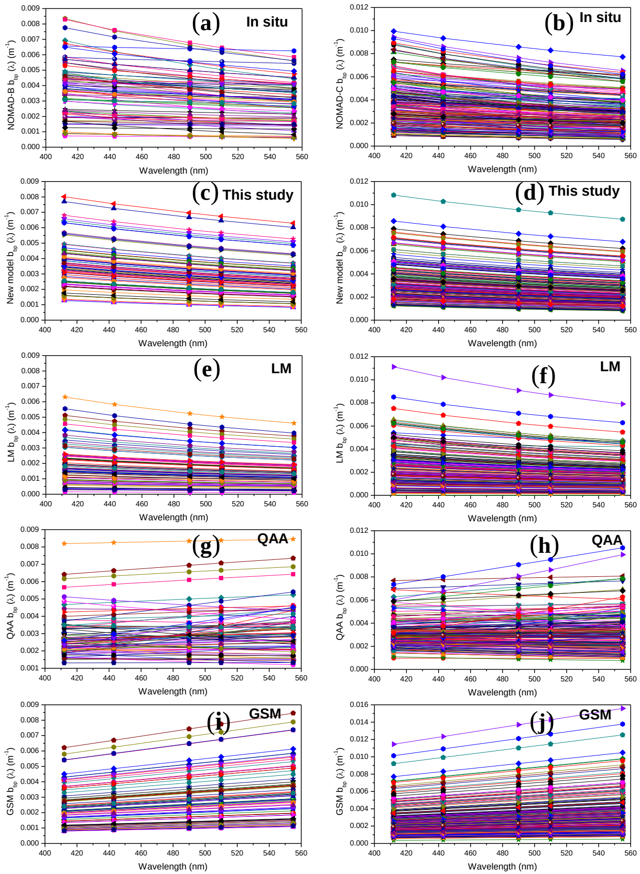

Fig. 6. Spectral variations in the particulate backscattering spectra $b_{bp}(\lambda)$ (m^{-1}) from the NOMAD-B data (left panel) and NOMAD-C (right panel) data (**a** and **b**) and from the four inversion models **(c–j)**.

OSD
10, 261–290, 2013

CC BY

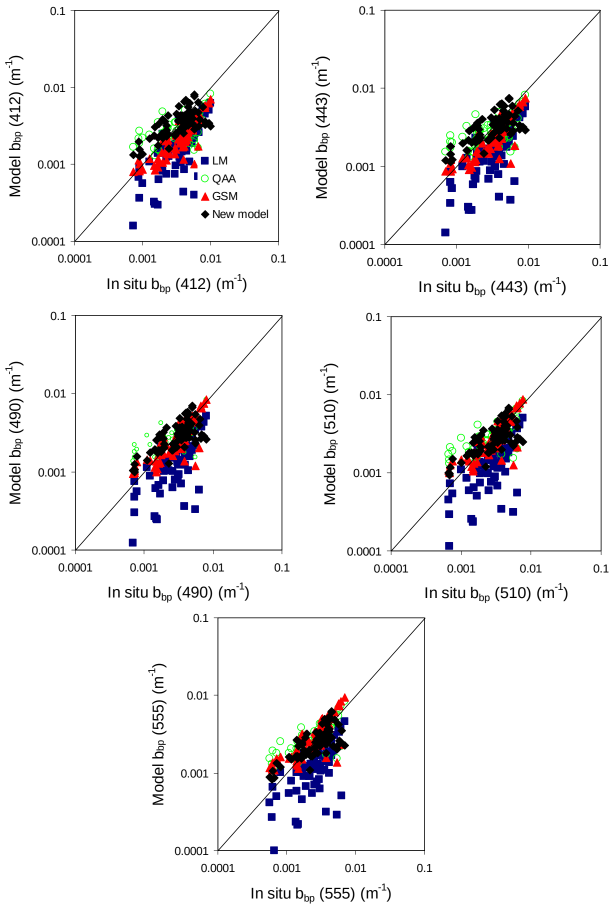

Fig. 7. Comparisons between the model $b_{bp}(\lambda)$ (m^{-1}) (from NOMAD SeaWiFS R_{rs} match-ups data set) and NOMAD-B in-situ data at the wavelengths from 412 to 555 nm ($N = 74$).

OSD
10, 261–290, 2013

Spectral particulate backscattering coefficients

S. P. Tiwari and P. Shanmugam

CC BY

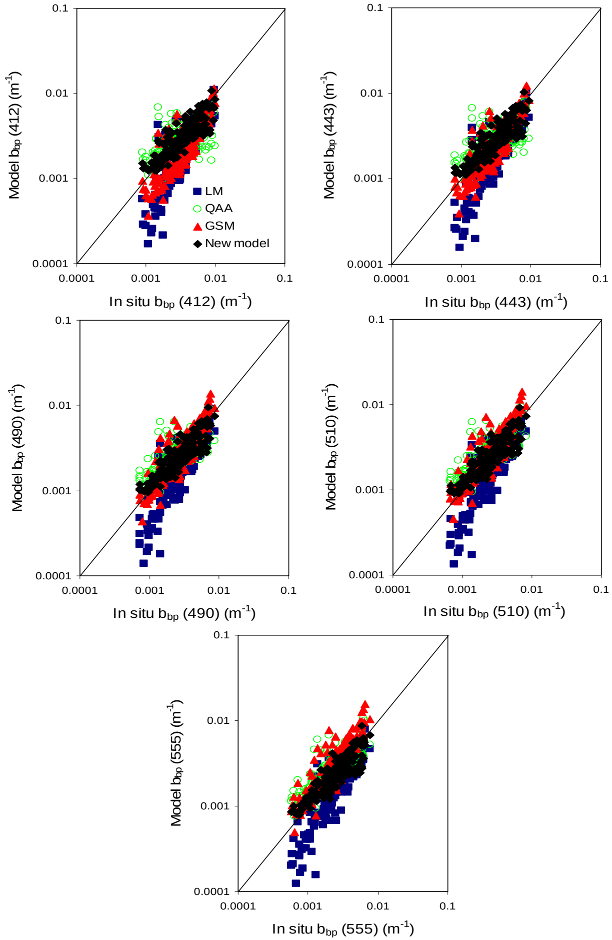

Fig. 8. Comparisons between the model $b_{bp}(\lambda)$ (m^{-1}) and NOMAD-C in-situ data at the wavelengths from 412 to 555 nm (N = 185).

CC BY